Asymmetric dimethylation amplifies stress granule assembly via phase separation

Ke Ruan (kruan@ustc.edu.cn)
University of Science and Technology of China https://orcid.org/0000-0001-9358-0451

Weiwei Fan

Mengtong Qin
University of Science and Technology of China

Feng Chen
University of Science and Technology of China https://orcid.org/0000-0002-0182-5712

Linge Li
University of Science and Technology of China

Tian Xu
University of Science and Technology of China

Hanyu Zhang
University of Science and Technology of China

Yan Li
University of Science and Technology of China

Duo-Duo Hu
University of Science and Technology of China

Shuaixin Gao
Center for Precision Medicine Multi-Omics Research, Peking University Health Science Center, Peking University

Ru Li
Tsinghua University

Jingwen Li
National Facility for Protein Science in Shanghai, Zhangjiang Lab, Shanghai Advanced Research Institute, Chinese Academy of Science

Weiqian Wang
National Facility for Protein Science in Shanghai, Zhangjiang Lab, Shanghai Advanced Research Institute, Chinese Academy of Science

Zhang Hai
USTC

Jia Gao
University of Science and Technology of China

Xing Liu

University of Science and Technology of China https://orcid.org/0000-0002-7480-5085
Xiaoming Tu
University of Science and Technology of China
Jihui Wu
University of Science and Technology of China
Wei He
Cancer Hospital of the First Affiliated Hospital of Zhengzhou University
Pilong Li
Beijing Advanced Innovation Center for Structural Biology, Beijing Frontier Research Center for Biological Structure, Tsinghua-Peking Joint Center for Life Sciences, School of Life Sciences, Tsinghu
https://orcid.org/0000-0002-1783-3100
Xuebiao Yao
University of Science and Technology of China https://orcid.org/0000-0001-8982-5911
Catherine Wong
Center for Precision Medicine Multi-Omics Research, Peking University https://orcid.org/0000-0002-6855-2798
Yunyu Shi
University of Science and Technology of China
Xi-Sheng Wang
University of Science and Technology of China
Zhong-Huai Hou
University of Science and Technology of China
Zhenye Yang
University of Science and Technology of China https://orcid.org/0000-0001-7797-5891
Dan Liu
University of Science and Technology of China

Article

Keywords:

Posted Date: March 17th, 2022

DOI: https://doi.org/10.21203/rs.3.rs-1233936/v1

Abstract

Stress granules (SGs) form through phase separation of biomacromolecules to assist cells in resisting environmental stresses. Numbers of SG proteins contain Arg-Gly-Gly (RGG) motifs, indicating their RNA binding ability, and providing a substrate platform for asymmetric dimethylation of arginine (ADMA), whose roles in SG assembly remain unclear. Here, we demonstrated that Caprin1-mediated recruitment of PRMT1 asymmetrically dimethylates RGGs to provide multiple binding sites for TDRD3, a typical ADMA reader, which in turn bridges the multivalent interactions between RGG motifs and RNA to promote phase separation. This process was suppressed by a bivalent inhibitor of TDRD3, eventually inhibiting proliferation more effectively than arsenite treatment alone. Our work reveals the role of ADMA in SG assembly and the potential of targeting condensates for cancer therapy.

Main Text

Ribonucleoprotein (RNP) granules spatiotemporally coordinate numbers of simultaneous biochemical reactions by compartmentalization of biomacromolecules[1]. Unlike those of the nucleus, stress granules (SGs) in the cytosol form through liquid–liquid phase separation (LLPS) when cells are exposed to environmental stresses, e.g., chemotherapy, heat shock, or osmotic shock[2–6]. Under this condition, various biomacromolecules, including translation initiation factors, RNA-binding proteins (RBPs), RNA, etc.[7–9], condense in cells, accompanied by mRNA translation arrest, to resist external environmental stresses [4, 10, 11]. The dysregulation of SG assembly, driven by multivalent interactions between RBPs and RNA [8, 12–14], induces a pathological liquid-solid phase transition, which eventually is closely related to various diseases, e.g., neurodegenerative diseases, infectious diseases and cancers [6, 7, 15, 16].

Posttranslational modifications have been nominated as economical regulators of RNP granule formation, as they can directly mediate the multivalent interactions between macromolecules, thus can enrich or exclude the modified macromolecules and/or their binding partner into or from condensates[10, 17]. A previous study identified 411 proteins as SG components [7], and approximately 20% of these proteins contained at least one Arg-Gly-Gly (RGG) motifs motif, double the percentage of RGG motif-containing proteins across the whole genome as determined in the UniProt database (Fig. 1a). Intriguingly, 82% of these RGG-containing proteins act as RBPs. RGG is a typical substrate motif for asymmetric dimethylation of arginine (ADMA), which is confirmed to be important in SG assembly[1, 18–20].

Protein arginine methyltransferase 1 (PRMT1) mediates > 85% of asymmetric dimethylation of arginine (ADMA) activity in cells [21, 22]. Arginine methylation does not always suppress the granule formation, despite the fact that arginine methylation directly weakens the protein-RNA interactions and thus suppresses LLPS in vitro [23]. Thus, the general roles of ADMA in SG components, especially RGG-containing RBPs, urgently need to be elaborated clearly.

Results

Caprin1 recruits PRMT1 to stress granules

By using Flag-tagged PRMT1 as bait, we identified large amounts of PRMT1-associated proteins (Extended Data Fig. 1a) by coimmunoprecipitation and mass spectrometry in HEK293T cells treated with arsenite, which is usually used to mimic stress conditions. A large proportion of PRMT1-associated proteins were SG components, including G3BP1 and Caprin1 (Fig. 1b). Subsequent dual immunofluorescence staining of endogenous PRMT1 and each of two recognized SG proteins, G3BP1 and eIF3η [24], was performed and confirmed that PRMT1 was preferentially localized in the SGs of arsenite-stressed U2OS cells (Extended Data Fig. 1b). Knocking down PRMT1 by siRNA in U2OS cells significantly reduced the fluorescence intensity of G3BP1 and the phase-separated SG area represented by G3BP1 (Fig. 1c-e; Extended Data Fig. 1c). These results indicate that endogenous PRMT1 is localized as a stable component in SGs in stressed cells and plays important roles in SG formation.

The mechanism of PRMT1 recruitment to SGs remains unclear. Based on the results of our immunoprecipitation assay and a previous study [2, 15], we selected nine SG proteins, including Caprin1 and G3BP1, which have been identified as core constituent proteins of SGs. By coexpressing these proteins with mEGFP-tagged and mCherry-tagged PRMT1 in arsenite-treated U2OS cells, we surprisingly observed that only in cells with Caprin1 expression did mCherry-tagged PRMT1 localize to SGs (Extended Data Fig. 1d). Moreover, knocking down endogenous Caprin1 in stressed U2OS cells (hereafter referred to as Caprin1 KO cells) by using the CRISPR/Cas9 system led to a drastic reduction in endogenous PRMT1 in SGs (Fig. 1f-g; Extended Data Fig. 1e). In addition to this phenomenon, both the fluorescence intensity of G3BP1 in SGs and the phase-separated SG area represented by G3BP1 were greatly decreased (Fig. 1h,i) in arsenite-stressed U2OS cells lacking Caprin1. Furthermore, our coimmunoprecipitation assay verified the coexistence of PRMT1 and Caprin1 in the same complex in stressed cells (Extended Data Fig. 1f). Combining these results, we concluded that Caprin1 stably associates with PRMT1 and recruits PRMT1 into SG condensates in stressed cells.

Asymmetric dimethylation of RGGs maintains stress granule integrity

The presence of typical RGG motifs in Caprin1 prompted us to carry out domain mapping to determine the specific domain responsible for PRMT1 recruitment. Mutants with truncation of four domains of Caprin1, the HR1, E-rich, HR2, and C-terminal (CT, residues 607–709; RGG-enriched) domains, were generated[25, 26]. When these mEGFP-tagged truncations were expressed in U2OS cells, CT-deleted Caprin1 failed to localize mCherry-tagged PRMT1 to SGs (Fig. 2a). Consistent with this result, when each of the four domains was expressed separately in U2OS cells, mCherry-PRMT1 was localized in SGs only in cells with CT domain expression (Extended Data Fig. 2a). Subsequent coimmunoprecipitation assays further confirmed that the CT domain of Caprin1 interacts with PRMT1 in cells, while truncated Caprin1 lost this ability, indicating that the CT domain of Caprin1 plays a core role in PRMT1 recruitment (Extended Data Fig. 2b). GST pulldown assays further revealed that the Caprin1 CT domain interacts with PRMT1 directly, with much higher affinity than that for G3BP1, the core component of SG assembly (Extended Data Fig. 2c), which provides evidence that Caprin1 plays key roles in recruiting PRMT1 to SGs.

The CT domain of Caprin1 contains three RGG motifs (R612, R633, and R690). First, we confirmed that ADMA does occur at these three sites in stressed cells by enrichment of HA-tagged Caprin1 through immunoprecipitation in arsenite-treated HEK293T cells and subsequent mass spectrometry analysis (Extended Data Fig. 2d,e). Next, we mutated these three arginines to alanine (A) or lysine (K) to generate the R612A/K, R633A/K, R690A/K, R612/633/690A (R/A 3) and R612/633/690K (R/K 3) constructs of Caprin1, which we then expressed in U2OS cells to observe whether these mutations affect PRMT1 accumulation in SGs in stressed cells. The results showed that in Caprin1 R612A-, R/A 3-, and R/K 3-expressing cells, PRMT1 failed to enter SGs in arsenite-stressed cells (Fig. 2b,c; Extended Data Fig. 2f). Subsequent coimmunoprecipitation assays confirmed that these three mutants had a weakened association with Flag-PRMT1 in HEK293T cells (Extended Data Fig. 2g). Furthermore, we verified these results through rescue experiments. Reconstitution of wild-type HA-Caprin1 in Caprin1 KO cells restored PRMT1 localization in SGs and significantly enhanced both the fluorescence intensity of G3BP1 in SGs and the phase-separated SG area represented by G3BP1, while reconstitution of Caprin1 with the R/A 3 mutant failed to rescue these phenotypes (Fig. 2d-f; Extended Data Fig. 2h). Since mutation of arginine (R) to lysine (K) maintains the charge of the amino acid, while mutation of arginine (R) to alanine (A) alters the charge density, these results suggest that PRMT1 promotes asymmetric dimethylation of these three RGG motifs to play important roles in accumulating PRMT1 in SGs, which is essential for integrated SG formation.

G3BP1 has been suggested to be a core initiator of SG phase separation [2, 3] and to interact with Caprin1 directly [27, 28]. This observation prompted us to select it as our focus of further research on RGG-containing RBPs within SGs. To assess variations in the arginine methylation level in the G3BP1 RGG motifs (R435 and R447) under stress conditions, we transfected Flag-G3BP1 into U2OS cells and treated the cells with arsenite. At 0, 30, and 60 minutes after arsenite addition, we harvested cells and enriched G3BP1 by immunoprecipitation with an anti-Flag antibody; we then stained the cells with an anti-ADMA antibody. Clearly, the G3BP1 methylation level was increased gradually by arsenite treatment in a time-dependent manner and was decreased after arsenite washout (Fig. 2g). As a control, the RGG mutant (R435/447A) of G3BP1 exhibited marked depletion of methylation. Intriguingly, the upregulation of methylation was synchronized with the formation of SGs, as determined by the expression of endogenous TDRD3, which is an ADMA reader, and G3BP1 (Fig. 2h). Additionally, expression of wild-type TDRD3 greatly enhanced SG assembly (Extended Data Fig. 2i,j). A previous study identified TDRD3 as an SG-associated protein [29]. Our results confirm this observation and suggest that TDRD3 is possibly recruited by methylated RGGs and participates in phase separation-dependent SG assembly.

TDRD3 promotes LLPS of methylated RGGs with RNAs

To reveal the underlying mechanism, we performed in vitro phase separation assays based on the ternary system composed of G3BP1, TDRD3 and total RNA, herein referred to as the G3BP1-TDRD3-RNA system. First, the phase separation of the G3BP1 RRM-RGG (residues 327 to 466) was significantly promoted by total RNA extracted from HeLa cells (Fig. 3a). The residue-by-residue chemical shift perturbations (CSPs) of ^{15}N-labeled RRM-RGG induced by short RNA sequences suggested F382 and N346 as key residues for

RNA binding (Extended Data Fig. 3a,b). The results of mutagenesis suggested that both the RRM and RGG contribute to the RNA-mediated phase separation tendency of G3BP1 (Extended Data Fig. 3c). However, the LLPS capacity was dramatically reduced by the methylated G3BP1 RRM-RGG, which was purified after coexpression with PRMT1 in *E. coli* (Fig. 3b). Intriguingly, the TDRD3 Tudor domain fully restored and even further promoted the phase separation of the methylated G3BP1-TDRD3-RNA system (Fig. 3b). Moreover, the CT of Caprin1 resulted in similar effects, indicating that RGG-containing proteins in stress granules may share this property (Extended Data Fig. 3d-e).

We then mapped the binding topology of methylated G3BP1 and TDRD3. As R435 and R447 in the G3BP1 RRM-RGG are sites of PRMT1-mediated methylation in cells [19], we determined the residue-by-residue CSPs of the ^{15}N-labeled TDRD3 Tudor domain induced by a chemically synthesized asymmetrically dimethylated R447 (R447^{me2a}: GPPR^{me2a}GGMVQK) peptide. The G3BP1 R447^{me2a} peptide bound to the aromatic cage of the TDRD3 Tudor domain (Extended Data Fig. 3f,g). Accordingly, the methylated G3BP1 RRM-RGG domain bound to the same aromatic cage, as highlighted by the similar CSP pattern of TDRD3 (Fig. 3c). Recognition of methylated arginine by TDRD3 is key to the liquid–liquid phase separation (LLPS) of the G3BP1-TDRD3-RNA system, as blockade of this interaction by the TDRD3 N596A mutation (Fig. 3c and Extended Data Fig. 3g) suppressed liquid droplet formation in vitro (Extended Data Fig. 3h) and in cells (Extended Data Fig. 3i,j). The TDRD3 Tudor domain also binds to RNA at sites other than the aromatic cage (Fig. 3d); thus, we concluded that TDRD3 bridges the interactions between RNA and methylated G3BP1.

The aforementioned studies imply that the phase separation of the methylated G3BP1-TDRD3-RNA system could be chemically mediated by disrupting the interactions between the TDRD3 aromatic cage and methylated RGGs in G3BP1. Two inhibitors (**iTud** and **B**), which had the highest binding affinities for the TDRD3 aromatic cage among the hits identified from previous fragment screening [30], suppressed the LLPS of the methylated G3BP1-TDRD3-RNA system in a dose-dependent manner (Fig. 3e). The fluorescence recovery after photobleaching assay demonstrated that the unmethylated G3BP1-TDRD3-RNA system had a higher fluidity than the methylated G3BP1-TDRD3-RNA system and that this fluidity was restored by the addition of inhibitor **iTud** (Fig. 3f,g). These results indicate that the involvement of TDRD3 promotes SG phase separation by mediating the interactions between methylated RGGs and RNA. Methylated RGGs accumulate TDRD3 Tudor domains, which contain multiple RNA binding sites, to agglutinate more RNA and thus enhance multivalent interactions within condensates in cells to facilitate the formation of integrated SGs.

TDRD3 recruited by methylated RGGs enhances multivalent interactions within condensates

To confirm this idea, we generated tandem Tudor chimeras (TTCs) and found that the TTCs more strongly promoted the phase separation tendency of the G3BP1-TTC-RNA system than the G3BP1-TDRD3-RNA system (Fig. 4a), confirming that the valence enhancement provided by RGG methylation in SG condensates establishes a recruiting platform of TDRD3 for RNA agglutination. A single TDRD3 Tudor domain bound to the R447^{me2a} or R435^{me2a} peptide with an affinity not greater than 0.35 ± 0.01 mM

(fitting error), while the TTC exhibited an enhanced affinity of 0.16 ± 0.01 mM (fitting error) for the R435^{me2a}/R447^{me2a} peptide (Extended Data Fig. 4a-c). The R435^{me2a}/R447^{me2a} peptide suppressed the LLPS of the methylated G3BP1-TDRD3-RNA system via competitive interactions between methylated RGGs and the Tudor domain more effectively than did its counterpart with a single methylation site (Extended Data Fig. 4d). We further synthesized a bivalent inhibitor (**BiTud**) by linking two **iTud** molecules together to achieve higher affinity and better cell penetration (Extended Data Fig. 4e). **BiTud** bound to TDRD3 TTC with an affinity of 5 ± 1 μM (Fig. 4b), while compound **iTud** exhibited an affinity of 66 μM for the TDRD3 single Tudor domain. Accordingly, **BiTud** suppressed the LLPS of the methylated G3BP1-TDRD3-RNA system in vitro (Fig. 4c,d) and inhibited cellular SG assembly at lower concentrations than compound **iTud** alone (Fig. 4e,f and Extended Data Fig. 4f). Furthermore, the combination of **BiTud** and arsenite strikingly suppressed the proliferation of U2OS cells in comparison with that after either treatment alone (Extended Data Fig. 4g), suggesting that **BiTud** sensitizes U2OS cells to arsenite treatment by inhibiting SG assembly, a potential mechanism of drug resistance.

Multiscale coarse-grained simulation verifies multivalent interactions in G3BP1-TDRD3-RNA system

A multiscale coarse-grained simulation was hence generated to further our understanding of LLPS of the G3BP1-TDRD3-RNA system driven by multivalent interactions. The flexible RNA and G3BP1 RGG region were coarse-grained into nucleotide- or residue-based models, respectively (Fig. 5a). The folded G3BP1 RRM domains and TDRDs were modeled as rigid patchy colloids, where the surface was annotated by interaction sites that were identified from NMR CSPs (Extended Data Fig. 3a and Fig. 3d). Four different conditions, corresponding to the unmethylated G3BP1-RNA system, methylated G3BP1-RNA system, methylated G3BP1-TDRD3-RNA system and unmethylated G3BP1-TDRD3-RNA system, were simulated at various G3BP1 concentrations (Fig. 5b). The cluster size when the equilibrium configurations were reached was analyzed as a quantitative indicator of the LLPS capability (Fig. 5c). The trend in the cluster size agreed well with the experimental LLPS data. Clearly, the methylated G3BP1-TDRD3-RNA system tended to form a highly condensed phase (Fig. 5d). The snapshots acquired during the coarse-grained simulation were statistically evaluated to determine the valence, defined as the number of binding RNA chains per G3BP1 molecule. The average valence thus represented the contacts in the G3BP1-RNA system at equilibrium. Although the G3BP1-RNA system valence was reduced by arginine methylation, the methylated arginine bound to TDRD3 and in turn recruited more RNA to reverse the valence loss (Fig. 5e). Trivalent interactions were predominantly present in the methylated G3BP1-TDRD3-RNA system, where the G3BP1 RRM and two TDRD3 Tudor domains each contacted a distinct RNA chain. The simulation results revealed the essential role of asymmetric dimethylation of arginine (ADMA) in RGGs during LLPS driven by multivalent interactions.

Taken together, our results reveal that Caprin1-mediated PRMT1 recruitment to SGs in stressed cells increases the likelihood of ADMA in SG proteins containing RGG motifs, which weakens the interactions of RBPs with RNA. Subsequent TDRD3 recruitment by methylated RGGs supplies more RNA binding sites, which hence amplifies SG assembly through phase separation (Fig. 5f). Intriguingly, suppression of SG

assembly through targeting ADMA suggests its indication in addressing the drug resistance in cancer therapy.

Declarations

Acknowledgments

Part of our study was performed at the National Center for Protein Science Shanghai and the Steady High Magnetic Field Facility of Chinese Academy of Sciences. We thank the National Key R&D Program of China (2019YFA0508400, 2021YFF0701700, 2016YFA0500702), the National Natural Science Foundation of China (32090042, 21874123, 31870760, 32090044, 21833007, 32090041, 21778050), the Collaborative Innovation Program of Hefei Science Center, CAS (2020HSC-CIP009), the Anhui Provincial Natural Science Foundation (2108085J12), the Fundamental Research Funds for the Central Universities (YD9100002011) for financial support.

Author contributions

Conceptualization: PL, ZH, ZY, KR, DL.

Methodology: WF, MQ, FC, LL, TX, HZ, YL, DH, SG, RL, JL, WW, WH, JZ, JG, JW, XW, KR.

Investigation: WF, MQ, FC, LL, TX, HZ, YL, DH, SG, XW.

Visualization: WF, MQ, FC, LL, TX, SG.

Funding acquisition: XL, XY, CW, YS, XW, ZH, ZY, KR, DL.

Project administration: XW, ZH, ZY, KR, DL.

Supervision: XL, XT, JW, PL, XY, CW, YS, XW, ZH, ZY, KR, DL.

Writing – original draft: WF, MQ, FC, LL, TX, SG.

Writing – review & editing: XY, XW, ZH, ZY, KR, DL.

Competing interests

Authors declare that they have no competing interests.

Data and materials availability

All data are available in the main text or the supplemental information.

References

1. Boeynaems, S. *et al.* Protein Phase Separation: A New Phase in Cell Biology. *Trends Cell Biol* 28, 420-435 (2018).

2. Yang, P. *et al.* G3BP1 Is a Tunable Switch that Triggers Phase Separation to Assemble Stress Granules. *Cell* **181**, 325-345 e328 (2020).

3. Sanders, D.W. *et al.* Competing Protein-RNA Interaction Networks Control Multiphase Intracellular Organization. *Cell* **181**, 306-324 e328 (2020).

4. Hofmann, S., Kedersha, N., Anderson, P. & Ivanov, P. Molecular mechanisms of stress granule assembly and disassembly. *Biochim Biophys Acta Mol Cell Res* **1868**, 118876 (2021).

5. Wallace, E.W. *et al.* Reversible, Specific, Active Aggregates of Endogenous Proteins Assemble upon Heat Stress. *Cell* **162**, 1286-1298 (2015).

6. Arimoto-Matsuzaki, K., Saito, H. & Takekawa, M. TIA1 oxidation inhibits stress granule assembly and sensitizes cells to stress-induced apoptosis. *Nat Commun* **7**, 10252 (2016).

7. Jain, S. *et al.* ATPase-Modulated Stress Granules Contain a Diverse Proteome and Substructure. *Cell* **164**, 487-498 (2016).

8. Markmiller, S. *et al.* Context-Dependent and Disease-Specific Diversity in Protein Interactions within Stress Granules. *Cell* **172**, 590-604 e513 (2018).

9. Van Treeck, B. & Parker, R. Emerging Roles for Intermolecular RNA-RNA Interactions in RNP Assemblies. *Cell* **174**, 791-802 (2018).

10. Panas, M.D., Ivanov, P. & Anderson, P. Mechanistic insights into mammalian stress granule dynamics. *J Cell Biol* **215**, 313-323 (2016).

11. Ivanov, P., Kedersha, N. & Anderson, P. Stress Granules and Processing Bodies in Translational Control. *Cold Spring Harb Perspect Biol* **11** (2019).

12. Riback, J.A. *et al.* Stress-Triggered Phase Separation Is an Adaptive, Evolutionarily Tuned Response. *Cell* **168**, 1028-1040 e1019 (2017).

13. Deniz, A.A. Networking and Dynamic Switches in Biological Condensates. *Cell* **181**, 228-230 (2020).

14. Riback, J.A. *et al.* Composition-dependent thermodynamics of intracellular phase separation. *Nature* **581**, 209-214 (2020).

15. Samir, P. *et al.* DDX3X acts as a live-or-die checkpoint in stressed cells by regulating NLRP3 inflammasome. *Nature* **573**, 590-594 (2019).

16. Silva, J.M. *et al.* Dysregulation of autophagy and stress granule-related proteins in stress-driven Tau pathology. *Cell Death Differ* **26**, 1411-1427 (2019).

17. Protter, D.S.W. & Parker, R. Principles and Properties of Stress Granules. *Trends Cell Biol* **26**, 668-679 (2016).

18. Hofweber, M. *et al.* Phase Separation of FUS Is Suppressed by Its Nuclear Import Receptor and Arginine Methylation. *Cell* **173**, 706-719 e713 (2018).

19. Tsai, W.C. *et al.* Arginine Demethylation of G3BP1 Promotes Stress Granule Assembly. *J Biol Chem* **291**, 22671-22685 (2016).

20. Chong, P.A., Vernon, R.M. & Forman-Kay, J.D. RGG/RG Motif Regions in RNA Binding and Phase Separation. *J Mol Biol* **430**, 4650-4665 (2018).

21. Tang, J. *et al.* PRMT1 is the predominant type I protein arginine methyltransferase in mammalian cells. *J Biol Chem* **275**, 7723-7730 (2000).

22. Nicholson, T.B., Chen, T. & Richard, S. The physiological and pathophysiological role of PRMT1-mediated protein arginine methylation. *Pharmacol Res* **60**, 466-474 (2009).

23. Roovers, E.F. *et al.* Tdrd6a Regulates the Aggregation of Buc into Functional Subcellular Compartments that Drive Germ Cell Specification. *Dev Cell* **46**, 285-301 e289 (2018).

24. Vonaesch, P., Campbell-Valois, F.X., Dufour, A., Sansonetti, P.J. & Schnupf, P. Shigella flexneri modulates stress granule composition and inhibits stress granule aggregation. *Cell Microbiol* **18**, 982-997 (2016).

25. Wu, Y., Zhu, J., Huang, X. & Du, Z. Crystal structure of a dimerization domain of human Caprin-1: insights into the assembly of an evolutionarily conserved ribonucleoprotein complex consisting of Caprin-1, FMRP and G3BP1. *Acta Crystallogr D Struct Biol* **72**, 718-727 (2016).

26. Kim, T.H. *et al.* Phospho-dependent phase separation of FMRP and CAPRIN1 recapitulates regulation of translation and deadenylation. *Science* **365**, 825-829 (2019).

27. Solomon, S. *et al.* Distinct structural features of caprin-1 mediate its interaction with G3BP-1 and its induction of phosphorylation of eukaryotic translation initiation factor 2alpha, entry to cytoplasmic stress granules, and selective interaction with a subset of mRNAs. *Mol Cell Biol* **27**, 2324-2342 (2007).

28. Kedersha, N. *et al.* G3BP-Caprin1-USP10 complexes mediate stress granule condensation and associate with 40S subunits. *J Cell Biol* **212**, 845-860 (2016).

29. Goulet, I., Boisvenue, S., Mokas, S., Mazroui, R. & Cote, J. TDRD3, a novel Tudor domain-containing protein, localizes to cytoplasmic stress granules. *Hum Mol Genet* **17**, 3055-3074 (2008).

30. Liu, J. *et al.* Structural plasticity of the TDRD3 Tudor domain probed by a fragment screening hit. *FEBS J* **285**, 2091-2103 (2018).

Figures

a

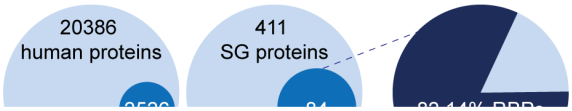

b

Gene	Peptide number		Gene	Peptide number	
	Flag-PRMT1	Flag-vector		Flag-PRMT1	Flag-vector
DDX1	40	6	*CAPRIN1*	12	0
DSP	27	1	*HSPA9*	12	13
DDX3X	21	4	*HNRNPA2B1*	12	2
RTCB	19	3	*SFPQ*	11	7

Figure 1

Caprin1 recruits PRMT1 to stress granules in stressed cells to accomplish SG assembly.

a, The proportions of RGG motif-containing proteins among 20386 human proteins and 411 SG proteins and the proportion of RBPs among the identified RGG motif-containing SG proteins. **b,** HEK293T cells were transfected with Flag-vector and Flag-PRMT1 separately. After arsenite treatment, a Co-IP experiment was performed, and the interacting protein networks of SG genes were identified by MS. **c-e,** U2OS cells transfected with the indicated siRNAs were treated with sodium arsenite (500 μM; 60 min) and stained for PRMT1 and G3BP1. Typical images are shown in **c**, The fluorescence intensity of G3BP1 in SGs and the SG area ratio (ratio of the G3BP1 area to the total cell area) were quantified in **d** and **e** respectively. Scale bar, 10 μm. The means ± SEMs (error bars) are shown. N≥20 cells per condition. **f-i,** Caprin1 KO cells were treated with sodium arsenite (500 μM; 60 min) and stained for PRMT1 and G3BP1. Typical images are shown in **f**. The fluorescence intensity of PRMT1 and G3BP1 in SGs and the SG area ratio (ratio of the G3BP1 area to the total cell area) were quantified in **g-i** respectively. Scale bar, 10 μm. The means ± SEMs (error bars) are shown. N≥20 cells per condition.

Figure 2

Asymmetric dimethylation of RGGs maintains stress granule integrity.

a, Viable U2OS cells were cotransfected with mEGFP-Caprin1 truncations and mCherry-PRMT1 and were then treated with sodium arsenite (500 μM; 60 min). Scale bar, 10 μm. **b,** U2OS cells were cotransfected with mEGFP-Caprin1 mutants in the C-terminal and mCherry-PRMT1 and were then treated with sodium

arsenite (500 µM; 60 min). **c,** Quantification of cells with PRMT1 in SGs. Scale bar, 10 µm. The means ± SEMs are shown (N≥15 cells per condition from two independent experiments). **d-f,** Caprin1 KO cells were transfected with HA-vector or HA-Caprin1 mutants, treated with sodium arsenite (500 µM; 60 min), and stained for HA, G3BP1 and PRMT1. Typical images are shown in **d,e**, and the SG area ratio (ratio of the G3BP1 area to the total cell area) was quantified in **f**. Scale bar, 10 µm. The error bars indicate the SEMs. **g,** Flag-G3BP1 and the methylation-deficient mutants R435A/R447A were transfected into U2OS cells. After treatment with arsenite (500 µM) for different times, asymmetric arginine methylation (ADMA) of the precipitated G3BP1 was detected with an antibody (upper panel), and the quantification of the ADMA intensity (lower panel) is shown. n = 3, Student's two-tailed t test. **h,** U2OS cells were treated with arsenite (500 µM) for different times and were then fixed and stained with DAPI (blue), an anti-TDRD3 antibody (red) and an anti-G3BP1 antibody (green). Scale bar, 20 µm.

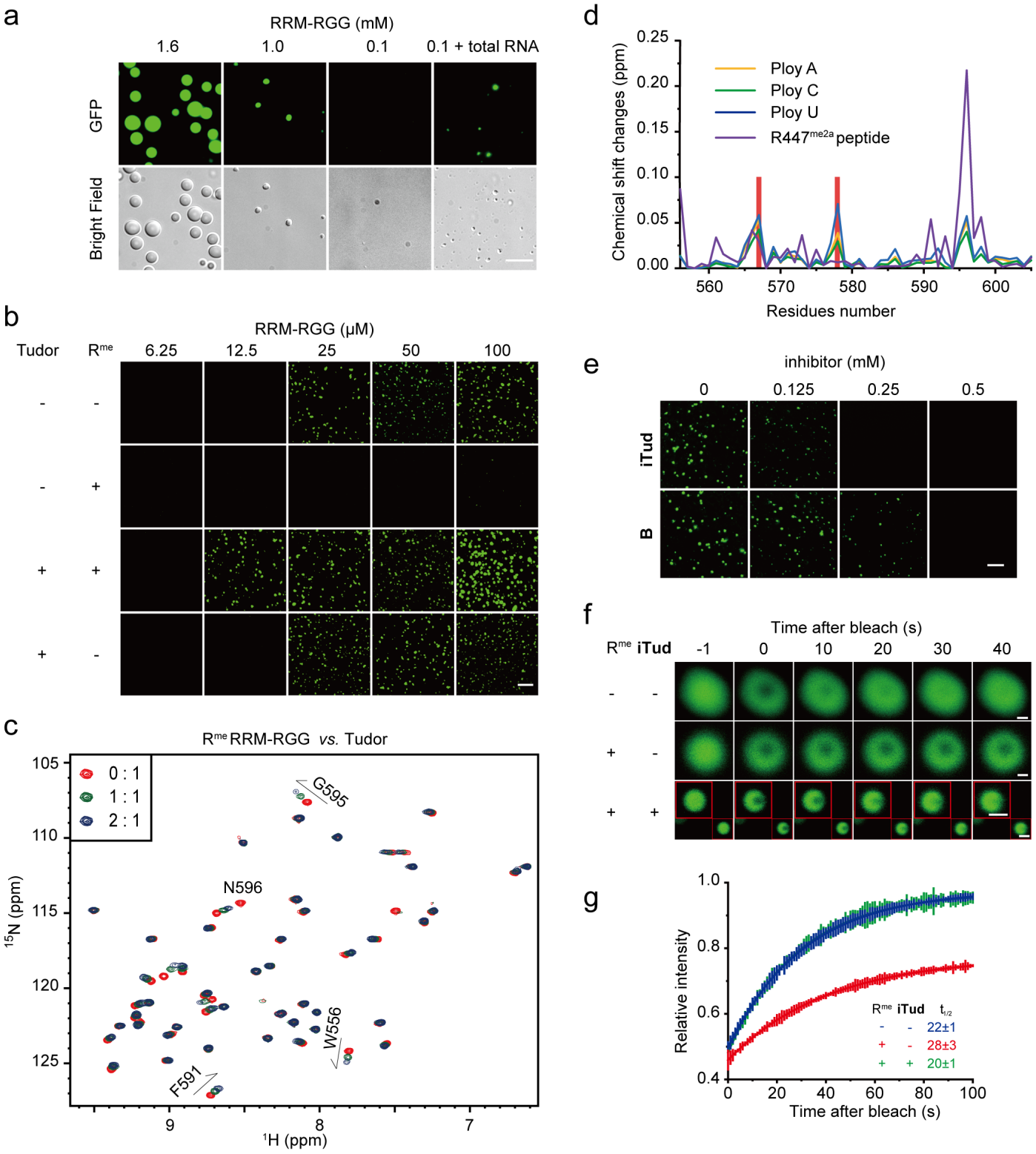

Figure 3

Methylated RGGs recruit TDRD3 to provide more RNA binding sites and promote G3BP1-based phase separation.

a, LLPS of the G3BP1 RRM-RGG with or without total RNA (20 ng/μL), which was extracted from HeLa cells. Images were acquired with a Nikon Eclipse Ti-E microscope. Scale bar, 10 μm. **b,** LLPS of the

methylated (R^{me}) or unmethylated G3BP1 RRM-RGG at different concentrations with or without the TDRD3 Tudor domain (50 μM). Total RNA, 20 ng/μL. Images were acquired with an LSM710 microscope (Zeiss). Scale bar, 20 μm. **c,** NMR chemical shift perturbation patterns of the TDRD3 Tudor domain titrated by methylated G3BP1 RRM-RGG. **d,** The chemical shift changes of the TDRD3 Tudor domain at a poly RNA (20 nt)/protein molar ratio of 2.0 or a peptide/protein molar ratio of 4.0. **e,** LLPS of the methylated G3BP1-TDRD3-RNA system was inhibited by compound **iTud** or **B**. RRM-RGG, 50 μM. Tudor, 50 μM. RNA, 20 ng/μL. Images were acquired with an LSM710 microscope (Zeiss). Scale bar, 20 μm. **f,** Fluorescence recovery after photobleaching (FRAP) assay of droplets formed by (un)methylated G3BP1-TDRD3-RNA with or without the inhibitor **iTud**. G3BP1 RRM-RGG, 50 μM. Tudor, 50 μM. Total RNA, 20 ng/μL. Images were acquired with an LSM710 microscope (Zeiss). Scale bar, 1 μm. **g,** Fitting curves show FRAP of different droplets. The error bars indicate the SEM of the biological duplicates.

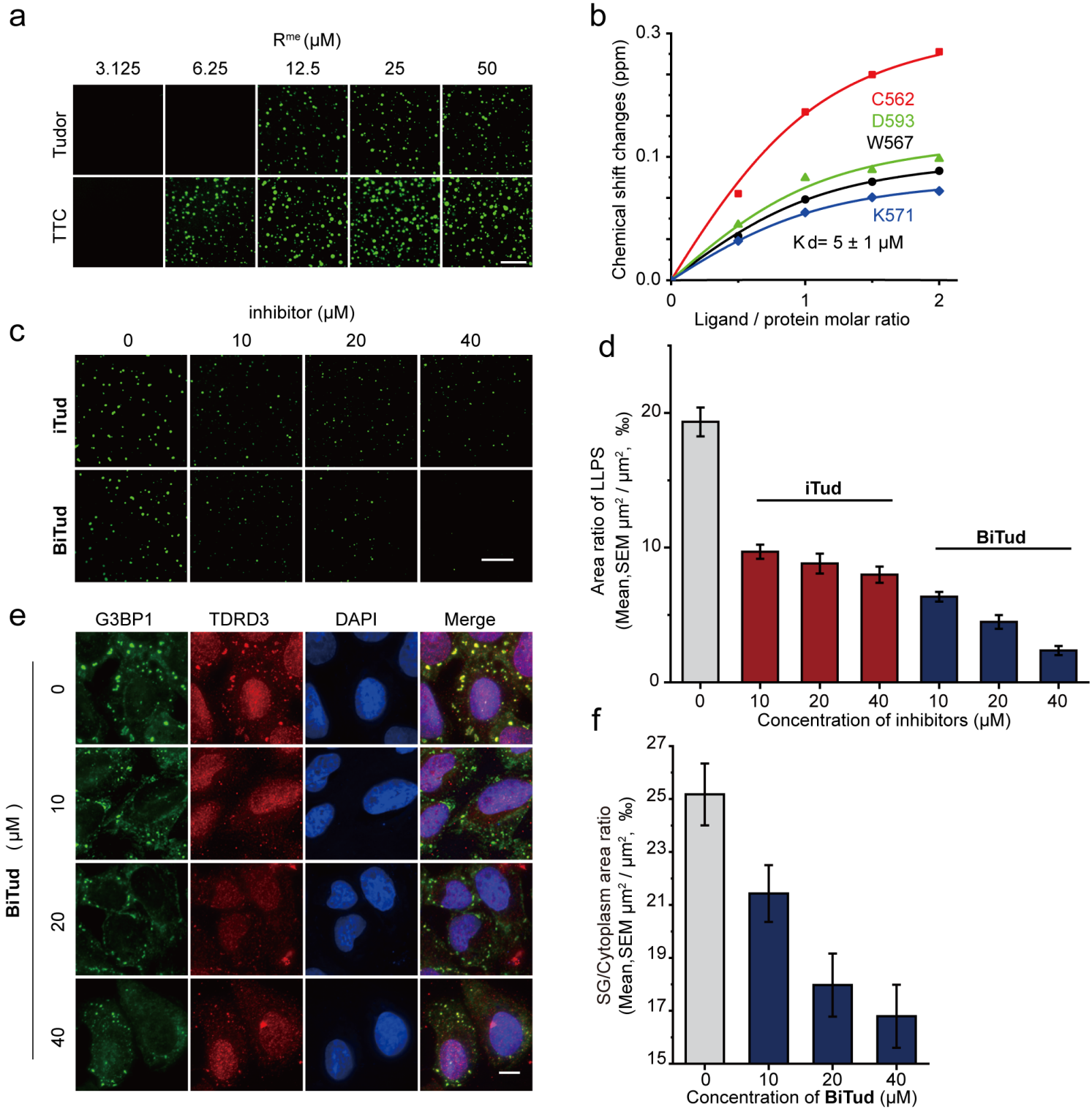

Figure 4

TDRD3-based valence enhancement induced by RGG methylation facilitates condensate formation.

a, LLPS of the methylated G3BP1 RRM-RGG (R^{me}) and RNA in the presence of a single TDRD3 Tudor domain (50 μM) or the tandem Tudor chimera (TTC, 25 μM). Total RNA, 20 ng/μL. Images were acquired with an LSM710 microscope (Zeiss). Scale bar, 20 μm. **b,** Fitting curves of the K_d value for binding between the inhibitor **BiTud** and the TTC determined from the dose-dependent NMR chemical shift

perturbations. TTC: 20μM. **c,** LLPS of the methylated G3BP1-TDRD3-RNA system was suppressed by the compound **iTud** or the bivalent inhibitor **BiTud**. G3BP1 RRM-RGG, 25 μM. TDRD3 Tudor, 25 μM. Images were acquired with an LSM710 microscope (Zeiss). Scale bar, 20 μm. **d,** Quantification of the area ratio of LLPS, n=16. **e,** U2OS cells were incubated with various concentrations of **BiTud** and were then treated with arsenite (500 μM) for 1 h. Cells were fixed and stained with DAPI (blue), an anti-TDRD3 antibody (red) and an anti-G3BP1 antibody (green). Images were acquired with a Nikon Eclipse Ti-E microscope. Scale bar, 10 μm. **f,** Quantification of the area ratio of SGs upon treatment with **BiTud**.

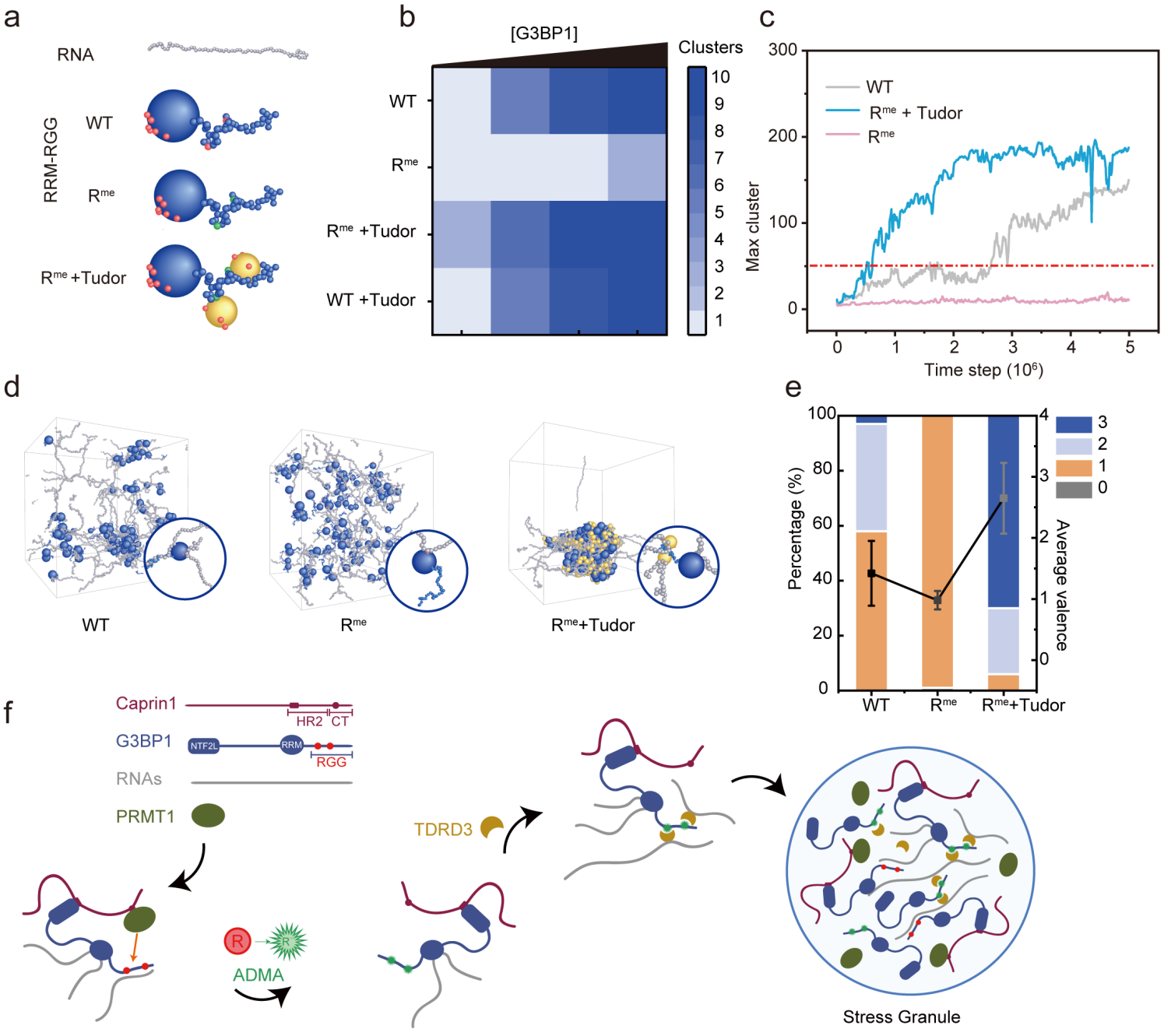

Figure 5

Multiscale coarse-grained simulation and the working model.

a, Schematic representation of the G3BP1-TDRD3-RNA model. The G3BP1 RGG region was simulated at a coarse-grained level, with each small blue sphere representing a residue, while the G3BP1 RRM (blue sphere) and TDRD3 Tudor domain (yellow sphere) were coarse-grained into rigid bodies. The red and silver spheres represent interaction sites and nucleotides, respectively. **b,** Equilibrium MD configurations of (un)methylated G3BP1-RNA in the absence or presence of the TDRD3 Tudor domain. **c,** Variation in the maximum cluster size by time step in the simulated systems. **d,** Simulation snapshots showing different valence conditions in which the specific protein contacts 1-3 RNA chains. **e,** Valence distributions and average valence of RNA contacts for each protein derived from the simulated ensemble. **f,** The working model of stress granule assembly mediated by arginine methylation on multiple RGGs.

Supplementary Files

This is a list of supplementary files associated with this preprint. Click to download.

- G3BP1SI202200217.docx
- FigS10217.tif
- FigS20217.tif
- FigS30217.tif
- FigS40217.tif